Acoustic analysis of anisotropic poroelastic multilayered systems

Article *in* Journal of Applied Physics · February 2016

DOI: 10.1063/1.4942443

4 authors:

Juan Pablo Parra Martinez
KTH Royal Institute of Technology
8 PUBLICATIONS **2** CITATIONS
SEE PROFILE

Olivier Dazel
Université du Maine
85 PUBLICATIONS **457** CITATIONS
SEE PROFILE

Peter Göransson
KTH Royal Institute of Technology
99 PUBLICATIONS **606** CITATIONS
SEE PROFILE

Jacques Cuenca
LMS International
48 PUBLICATIONS **190** CITATIONS
SEE PROFILE

AIP Journal of Applied Physics

Acoustic analysis of anisotropic poroelastic multilayered systems

Juan Pablo Parra Martinez, Olivier Dazel, Peter Göransson, and Jacques Cuenca

Citation: Journal of Applied Physics **119**, 084907 (2016); doi: 10.1063/1.4942443
View online: http://dx.doi.org/10.1063/1.4942443
View Table of Contents: http://scitation.aip.org/content/aip/journal/jap/119/8?ver=pdfcov
Published by the AIP Publishing

Acoustic analysis of anisotropic poroelastic multilayered systems

Juan Pablo Parra Martinez,[1,2,a)] Olivier Dazel,[2] Peter Göransson,[1] and Jacques Cuenca[1,3]
[1]*Centre for ECO²Vehicle Design & MWL, KTH Royal Institute of Technology, Teknikringen 8, SE-10044 Stockholm, Sweden*
[2]*Laboratoire d'Acoustique de l'Université du Maine - UMR CNRS 6613, Avenue Olivier Messiaen, F-72085 Le Mans Cedex, France*
[3]*Siemens Industry Software, Interleuvenlaan 68, B-3001 Leuven, Belgium*

(Received 27 November 2015; accepted 9 February 2016; published online 29 February 2016)

The proposed method allows for an extended analysis of the wave analysis, internal powers, and acoustic performance of anisotropic poroelastic media within semi-infinite multilayered systems under arbitrary excitation. Based on a plane wave expansion, the solution is derived from a first order partial derivative as proposed by Stroh. This allows for an in-depth analysis of the mechanisms controlling the acoustic behaviour in terms of internal powers and wave properties in the media. In particular, the proposed approach is used to highlight the influence of the phenomena intrinsic to anisotropic poroelastic media, such as compression-shear coupling related to the material alignment, the frequency shift of the fundamental resonance, or the appearance of particular geometrical coincidences in multilayered systems with such materials. © *2016 AIP Publishing LLC*.
[http://dx.doi.org/10.1063/1.4942443]

I. INTRODUCTION

It is well-known that most engineered poroelastic materials are inherently anisotropic due to the involved manufacturing processes,[1–5] and recent studies on multilayered finite-sized systems[6] have shown that anisotropy can significantly alter the dynamic behaviour of poroelastic materials. While the theoretical foundation for modelling anisotropic materials was established by Biot,[7–10] methods for efficiently predicting their vibro-acoustic behaviour within complex structures are still subject to research.

Recent progress on generally anisotropic materials includes finite element approaches,[11–15] and semi-analytical formulations for the analysis of seismic and electromagnetic waves.[16–18] However, to predict the physical phenomena governing the behaviour of finite-sized anisotropic porous media in multilayered configurations is still an open question. In such cases, the numerical modelling including poroelastic media involves a trade-off between complexity and computational efficiency. In particular, predicting the physical phenomena governing the behaviour of arbitrarily anisotropic porous media within multilayered configurations remains a challenge.

In addition, as a consequence of the lack of computational tools, the interpretation of the mechanical and energy-dissipating phenomena has not been systematically addressed for layers of finite thickness. For geophysical applications, the works by Carcione[18,19] discussed quadratic quantities associated with internal powers and energy propagation in the case of acoustic waves anisotropic porous media.

Regarding wave behaviour of multilayered systems including porous cores, Khurana *et al.*[20] extended the Transfer Matrix Method (TMM) for transversely isotropic porous materials by analytically solving the dispersion relation governing the wavenumbers of the waves travelling in the medium. Allard *et al.*[3] extended the research of the wave characteristics of transverse isotropic porous media whose plane of symmetry differs from the plane of incidence by applying a coordinate transformation but did not propose the transfer matrix for such media.

A TMM solution to the equations governing a fully anisotropic poroelastic medium has so far not been realised. Albeit theoretically tractable, this would lead to an eighth order algebraic equation in the wavenumbers, which has no known analytical solution. Furthermore, the derivation of the individual terms of the transfer matrix itself is prone to errors, and thus impractical.

The present paper proposes a method based on an expansion in plane waves, which forms the basis for a TMM model of the dynamics of a multilayered structure comprising arbitrarily anisotropic poroelastic layers. It allows for a detailed analysis of the mechanisms controlling the acoustic response of multilayered systems in terms of internal powers and wave properties in anisotropic poroelastic layers. The formulation consists in writing the equations governing the medium as a first order system in the selected state variables,[21–23] which appear in the boundary or coupling conditions between layers.

The paper is organised as follows. Sec. II introduces the plane wave solution and the governing equations in anisotropic poroelastic media. Sec. III presents the proposed approach to the calculation of quadratic quantities, such as dissipative and kinetic powers in the media. In Sec. IV, the application to a multilayer system including a layer of anisotropic poroelastic material is shown. An interpretation of the results in terms of waves is provided in Sec. V, where some aspects of the acoustic response are explained in terms of the kinetic powers and the dominant wave characteristics.

a)Electronic mail: jppm@kth.se

II. PLANE WAVE APPROACH FOR ANISOTROPIC POROUS MEDIA

A. General considerations

A multilayered system composed of homogeneous layers separating two semi-infinite fluid media is considered, as illustrated in Fig. 1, and where also the Cartesian coordinate system $\{0, x, y, z\}$ is defined. The system is excited by an incident acoustic plane wave of unit amplitude, positive in the z-direction, and defined by two angles θ_1 and θ_2 of incidence.

Throughout this paper, plane wave expansions are considered with a harmonic excitation at circular frequency ω. Hence, any dependent field variable $\hat{\chi}$ (e.g., displacement and stress) can be written as

$$\hat{\chi}(x, y, z, t) = \chi(z, \omega) e^{\imath(\omega t - k_x x - k_y y)}, \tag{1}$$

where $\chi(z, \omega)$ denotes the complex amplitude of the corresponding physical field and k_x and k_y are the components of the wave vector prescribed by the incident plane wave. As the spatial dependencies with respect to x and y, and the time dependence, are common to all fields and imposed by the incident wave, these will be omitted in order to simplify the expressions.

For an individual material layer, the amplitudes of the physical field variables required to describe its boundary or coupling conditions, form a state vector $\mathbf{s}(z)$. The remaining field amplitudes may be calculated as a linear combination of the fields in the state vector.

For any given individual layer, see Fig. 1, the linear equations of motion are written in terms of the state variables $\mathbf{s}(z)$ on the form, originally proposed by Stroh[21–23]

$$\frac{\partial \mathbf{s}(z)}{\partial z} = -\boldsymbol{\alpha}\, \mathbf{s}(z), \tag{2}$$

where $\boldsymbol{\alpha}$ is a square matrix that depends on the material parameters, the frequency, and the wavenumbers of the incident wave, k_x and k_y. The variation of the state variables along z is thus entirely governed by matrix $\boldsymbol{\alpha}$.

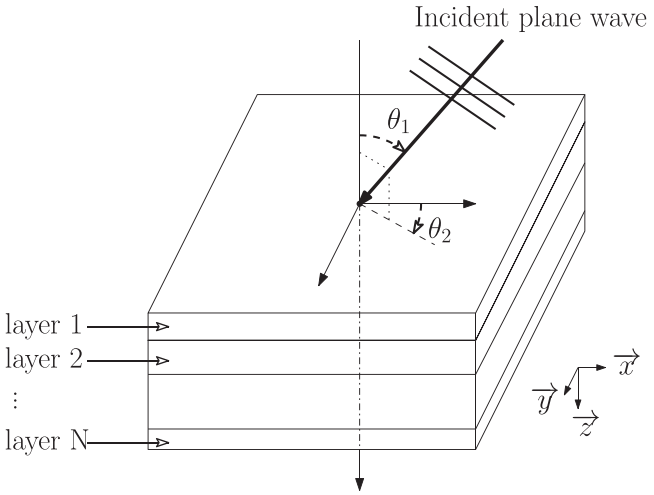

FIG. 1. Multilayered setup.

A direct solution of Eq. (2) may be obtained by integrating it over a distance $z - z_0$ smaller than the thickness of the layer, where z_0 is an arbitrary point in a layer. This leads to

$$\mathbf{s}(z) = \mathbf{M}(z, z_0)\, \mathbf{s}(z_0), \tag{3}$$

where $\mathbf{M}(z, z_0)$ is the transfer matrix of the medium between z and z_0. The latter depends on the constitutive parameters, such that

$$\mathbf{M}(z, z_0) = \mathbf{e}^{-(z - z_0)\boldsymbol{\alpha}}, \tag{4}$$

where $\mathbf{e}^{[\cdot]}$ is the matrix exponential operator.

A local coordinate system is introduced for each layer, aligned with the global coordinate system, with $z = 0$ at z_0.

An alternative way of expressing the transfer matrix may be obtained by a transformation into the eigenspace of Eq. (2). The eigenvalue problem for $\boldsymbol{\alpha}$ reads

$$\boldsymbol{\alpha} = \boldsymbol{\Phi}\boldsymbol{\Gamma}\boldsymbol{\Phi}^{-1}, \tag{5}$$

where $\boldsymbol{\Phi}$ and $\boldsymbol{\Gamma}$ are, respectively, a matrix whose columns are the eigenvectors and a diagonal matrix with the eigenvalues. Introducing a change of variables,

$$\mathbf{s}(z) = \boldsymbol{\Phi}\, \mathbf{w}(z) \tag{6}$$

and substituting this into Eq. (2) yields

$$\frac{\partial \mathbf{w}(z)}{\partial z} = -\boldsymbol{\Gamma}\, \mathbf{w}(z), \tag{7}$$

which is a system of uncoupled equations due to the diagonal nature of $\boldsymbol{\Gamma}$. The solution in the eigenspace can then be expressed as

$$\mathbf{w}(z) = \mathbf{e}^{-z\boldsymbol{\Gamma}} \mathbf{w}(0). \tag{8}$$

Transforming back to physical variables

$$\mathbf{s}(z) = \boldsymbol{\Phi} \mathbf{e}^{-z\boldsymbol{\Gamma}} \boldsymbol{\Phi}^{-1}\, \mathbf{s}(0), \tag{9}$$

which describes the wave propagation from 0 to z in terms of the eigenvectors and eigenvalues of $\boldsymbol{\alpha}$.

Rewriting Eq. (8) in the form

$$\mathbf{w}(z) = \boldsymbol{\Lambda}(z)\mathbf{q}, \tag{10}$$

where $\mathbf{q}$ is a vector containing the contribution of each wave in the layer, and $\boldsymbol{\Lambda}(z) = \mathbf{e}^{-\boldsymbol{\Gamma} z}$ describes the propagation in the layer, it follows that

$$\mathbf{s}(z) = \boldsymbol{\Phi}\boldsymbol{\Lambda}(z)\mathbf{q}. \tag{11}$$

The dimensions of $\boldsymbol{\Phi}$ and $\boldsymbol{\Lambda}(z)$ are $(n \times n)$, while $\mathbf{q}$ has dimension $(n \times 1)$, where n is the total number of waves existing in the medium.

Other wave properties which can be useful for the physical interpretation of the material behaviour, and that may be calculated from (5) are the wave slowness s_i, wave attenuation τ_i, and wavelength λ_i of the ith wave. Introducing $\imath k_{z,i} = \Gamma_i$ can be written as

$$s_i = \mathrm{Re}\left\{\frac{1}{V_i}\right\}, \tag{12}$$

$$\tau_i = -\omega\,\mathrm{Im}\left\{\frac{1}{V_i},\right\}, \tag{13}$$

$$\lambda_i = \mathrm{Re}\left\{\frac{2\pi}{k_{z,i}}\right\}, \tag{14}$$

where $V_i = \omega/k_{z,i}$ is the phase velocity of the ith wave.

From a known solution, the wave contributions, $\mathbf{q}$ can be determined by projecting the corresponding state variables in the eigenspace, as

$$\mathbf{q} = \mathbf{\Phi}^{-1}\,\mathbf{s}(0). \tag{15}$$

Up to this point, the derivations are applicable to any type of homogeneous media, both isotropic and anisotropic. The aim of the present work is to generalise the plane wave approach to the case of anisotropic poroelastic media with an arbitrary orientation of the incident wave.

B. Governing equations for a poroelastic layer

The porous material is modelled with the $\{\mathbf{u}^s, \mathbf{u}^t\}$ formulation proposed by Dazel *et al.*[24] The expressions for anisotropic open-cell poroelastic media are derived from the formulations in Hörlin and Göransson[13]

$$\nabla\cdot\hat{\boldsymbol{\sigma}}^s = -\omega^2\tilde{\boldsymbol{\rho}}_s\mathbf{u}^s - \omega^2\tilde{\boldsymbol{\rho}}_{eq}\tilde{\boldsymbol{\gamma}}\mathbf{u}^t, \tag{16}$$

$$-\nabla p = -\omega^2\tilde{\boldsymbol{\rho}}_{eq}\tilde{\boldsymbol{\gamma}}\mathbf{u}^s - \omega^2\tilde{\boldsymbol{\rho}}_{eq}\mathbf{u}^t, \tag{17}$$

$$\hat{\boldsymbol{\sigma}}^s = \hat{\mathbf{H}}^s\boldsymbol{\epsilon}^s, \tag{18}$$

$$p = -\tilde{K}_{eq}\nabla\cdot\mathbf{u}^t, \tag{19}$$

$$\mathbf{u}^t = \phi\,\mathbf{u}^f + (1-\phi)\,\mathbf{u}^s, \tag{20}$$

where $\mathbf{u}^s$ and $\mathbf{u}^f$, and $\mathbf{u}^t$ are, respectively, the vector of displacement fields of the solid and fluid phases, and the total displacement fields vector; $\boldsymbol{\epsilon}^s$ and $\boldsymbol{\sigma}^s$ are the porous solid Cauchy strain and stress vectors; and p is the acoustic pressure. The scalar quantities ϕ and $\tilde{K}_{eq}$ are, respectively, the porosity of the foam and the bulk modulus of the saturating fluid modified by the thermal exchanges with the solid phase of the porous medium.

The porous materials are here considered fully anisotropic, thus the complex terms $\tilde{\boldsymbol{\rho}}^s$, $\tilde{\boldsymbol{\rho}}^{eq}$, and $\tilde{\boldsymbol{\gamma}}$ are second order symmetrical tensors. $\hat{\mathbf{H}}^s$ is the Hooke's tensor of the solid phase of the material, which takes the form of a fourth order symmetrical tensor.[5] Furthermore, the porous medium is considered anelastic and is modelled by means of an augmented Hooke's law based on a fractional derivative approach[5,25]

The anisotropy is also reflected in the flow resistivity $\boldsymbol{\sigma}^{\mathrm{flow}}$, which is a second order symmetrical tensor, from which are derived several porous parameters, see Refs. 13, 20, 24, and 26 for isotropic media, which have been extended to anisotropic.[25]

To solve for the acoustic response under the plane wave assumption in Eq. (1), 8 independent amplitudes of the corresponding physical field variables are required. As indicated above, these are in the present work chosen from the coupling conditions for a specific porous layer, which in the present formulation involve continuity in the solid displacements (3 variables), the normal total displacement (1 variable), the surface solid normal traction (3 variables), and the acoustic pressure (a scalar quantity). Together these form the set of state variables

$$\begin{aligned}\mathbf{s}(z) = \{&u_x^s(z),\, u_y^s(z),\, u_z^s(z),\, u_z^t(z),\\ &\ldots\hat{\sigma}_{zz}^s(z),\, \hat{\sigma}_{yz}^s(z),\, \hat{\sigma}_{xz}^s(z),\, p(z)\}^{\mathrm{T}}.\end{aligned} \tag{21}$$

The remaining unknowns form a secondary set of variables

$$\mathbf{s}'(z) = \{u_x^t(z), u_y^t(z), \hat{\sigma}_{xx}^s(z), \hat{\sigma}_{yy}^s(z), \hat{\sigma}_{xy}^s(z)\}^{\mathrm{T}}. \tag{22}$$

C. Waves in anisotropic poroelastic media

In an isotropic poroelastic material, the Biot theory predicts four pairs of waves, namely, two compressional waves of different velocities (P1 and P2), and one shear wave with two perpendicular planes whose common axis is the propagation direction (S1 and S2). Similarly, for a transversally isotropic material, there are four pairs of waves which are polarised in such way that two quasi-compressional waves (qP1 and qP2), one quasi-shear wave (qS), and one shear wave (S) may be identified.

However, for a fully anisotropic porous material, there are in the general case 8 different waves that are neither characterised by compressional nor shear deformation,[19] as a wave can be polarised in any direction of space.

Thus, other means of wave classification are required. Here, the wave types controlling the response of a confined anisotropic porous medium are labelled following Eq. (11), as all 8 waves in the media have different wavenumbers, according to

$$\boldsymbol{\psi}_i = \boldsymbol{\phi}_i\,\Lambda_i, \quad i = 1,\ldots,8, \tag{23}$$

with $\boldsymbol{\phi}_i$ the eigenvector and $\boldsymbol{\Lambda}_i$ the eigenvalue of the ith wave.

A well known intricacy of wave propagation in anisotropic media is that, in Eq. (23), both $\boldsymbol{\phi}_i$ and $\boldsymbol{\Lambda}_i$ depend on direction of propagation as well as the orientation of the material alignment in space. As a consequence, there will be a different set of wave properties for each material orientation.

D. Matrix $\boldsymbol{\alpha}$ for anisotropic poroelastic media

One of the main contributions of the present work is the derivation of the $\boldsymbol{\alpha}$ matrix in Equation (2) corresponding to the state vector $\mathbf{s}(z)$ in Eq. (21), for a generally anisotropic poroelastic material.

As part of this, the linear relations between the variables in $\mathbf{s}'(z)$ and $\mathbf{s}(z)$ need to be established in order to calculate the partial derivatives of the fields in the state vector. Assuming the ordering of the fields in the state vector in Eq. (21), a numerical convention is used for the referencing of rows and columns in matrices. For a given matrix $\mathbf{R}|_{i:j}^{k:l}$, the subscripts refer to the lines i to j, and the superscripts refer to the columns k to l. The symbol [:] alone corresponds to all the elements in a row or column. An index alone corresponds to an individual row or column.

Before going into the details of the derivations, some straightforward Boolean operators will be defined.

The stress components appearing in the state variable vector are given by

$$\begin{Bmatrix} \hat{\sigma}_{zz}(z) \\ \hat{\sigma}_{yz}(z) \\ \hat{\sigma}_{xz}(z) \end{Bmatrix} = \mathbf{T}^{\hat{\boldsymbol{\sigma}}}\mathbf{s}(z), \tag{24}$$

where $\mathbf{T}^{\hat{\boldsymbol{\sigma}}}$ is the Boolean matrix defined as

$$\mathbf{T}^{\hat{\boldsymbol{\sigma}}} = \begin{bmatrix} 0\,0\,0\,0\,1\,0\,0\,0 \\ 0\,0\,0\,0\,0\,1\,0\,0 \\ 0\,0\,0\,0\,0\,0\,1\,0 \end{bmatrix}. \tag{25}$$

In a similar way, the solid displacement field components can be rewritten as a function of the state vector as

$$\mathbf{u}^s(s) = \mathbf{T}^{\mathbf{u}^s}\mathbf{s}(z), \tag{26}$$

where $\mathbf{T}^{\mathbf{u}^s}$ is defined by

$$\mathbf{T}^{\mathbf{u}^s} = \begin{bmatrix} 1\,0\,0\,0\,0\,0\,0\,0 \\ 0\,1\,0\,0\,0\,0\,0\,0 \\ 0\,0\,1\,0\,0\,0\,0\,0 \end{bmatrix}. \tag{27}$$

Finally, the pressure is given from the state variable vector as

$$p(z) = \mathbf{T}^p\mathbf{s}(z), \tag{28}$$

where the Boolean matrix is

$$\mathbf{T}^p = [0\,0\,0\,0\,0\,0\,0\,1]. \tag{29}$$

1. Gradient of solid displacements, $\frac{\partial}{\partial z}\mathbf{u}^s(z)$

To determine

$$\frac{\partial}{\partial z}\mathbf{u}^s(z) = \boldsymbol{\alpha}|_{1:3}^{:}\,\mathbf{s}(z), \tag{30}$$

the relation between the normal solid strain and the corresponding stress components will be derived. The Cauchy strain vector $\boldsymbol{\epsilon}^s(z)$, in Voigt notation, may be expressed as

$$\boldsymbol{\epsilon}^s(z) = \underbrace{\begin{bmatrix} -\imath k_x & 0 & 0 \\ 0 & -\imath k_y & 0 \\ 0 & 0 & 0 \\ 0 & 0 & -\imath k_y \\ 0 & 0 & -\imath k_x \\ -\imath k_y & -\imath k_x & 0 \end{bmatrix}}_{\mathbf{A}}\mathbf{u}^s(z) + \underbrace{\begin{bmatrix} 0 & 0 & 0 \\ 0 & 0 & 0 \\ 0 & 0 & 1 \\ 0 & 1 & 0 \\ 1 & 0 & 0 \\ 0 & 0 & 0 \end{bmatrix}}_{\mathbf{B}}\frac{\partial}{\partial z}\mathbf{u}^s(z). \tag{31}$$

Finally, to relate the stresses to the strains, Eqs. (25), (26), and (31) can be substituted into Eq. (18), such that the $\boldsymbol{\alpha}|_{1:3}^{:}$ is obtained as

$$\boldsymbol{\alpha}|_{1:3}^{:} = [\hat{\mathbf{H}}^s|_{3:5}^{:}\,\mathbf{B}]^{-1}[\mathbf{T}^{\hat{\boldsymbol{\sigma}}} - \hat{\mathbf{H}}^s|_{3:5}^{:}\,\mathbf{A}\mathbf{T}^{\mathbf{u}^s}]. \tag{32}$$

2. Gradient of total displacement, $\frac{\partial u_z^t(z)}{\partial z}$

In a similar manner, Eq. (19) provides the term $\partial u_z^t(z)/\partial z$ which is associated to the 4th row of $\boldsymbol{\alpha}$

$$\frac{\partial u_z^t(z)}{\partial z} = \boldsymbol{\alpha}|_4^{:}\,\mathbf{s}(z). \tag{33}$$

The Cartesian components of the total displacement fields $\mathbf{u}^t(z)$ may be obtained from Eq. (17) as

$$\mathbf{u}^t(z) = \frac{1}{\omega^2}[\tilde{\rho}^{eq}]^{-1}\nabla p(z) - \tilde{\boldsymbol{\gamma}}\mathbf{u}^s(z). \tag{34}$$

To express $\mathbf{u}^t(z)$ as a function of the state vector, the (3×8) matrix $\mathbf{T}^{\mathbf{u}^t}$ is introduced

$$\mathbf{u}^t(z) = \mathbf{T}^{\mathbf{u}^t}\mathbf{s}(z). \tag{35}$$

The z-component of the total displacement vector, $u_z^t(z)$, is given by the 4th field in $\mathbf{s}(z)$, and thus the 3rd row of $\mathbf{T}^{\mathbf{u}^t}$ is

$$\mathbf{T}^{\mathbf{u}^t}|_3^{:} = [0\,0\,0\,1\,0\,0\,0\,0], \tag{36}$$

and $u_x^t(z)$ and $u_y^t(z)$ from

$$\mathbf{T}^{\mathbf{u}^t}|_{1:2}^{1:2} = -\tilde{\boldsymbol{\gamma}}|_{1:2}^{1:2}, \tag{37}$$

and

$$\mathbf{T}^{\mathbf{u}^t}|_{1:2}^{8} = -[\tilde{\boldsymbol{\rho}}^{eq}]^{-1}|_{1:2}^{1:2}\begin{pmatrix} \imath k_x/\omega^2 \\ \imath k_y/\omega^2 \end{pmatrix}. \tag{38}$$

Thus, using Eqs. (29) the 4th row of $\boldsymbol{\alpha}$ may be expressed as

$$\boldsymbol{\alpha}|_4^{:} = -\frac{1}{\tilde{K}_{eq}}\mathbf{T}^p + \imath k_x\mathbf{T}^{\mathbf{u}^t}|_1^{:} + \imath k_y\mathbf{T}^{\mathbf{u}^t}|_2^{:}. \tag{39}$$

3. Gradient of Cauchy stresses, $\frac{\partial}{\partial z}\hat{\sigma}_{iz}^s$, for $i = z, y, x$

The partial derivative over z of the solid stress components in the $\mathbf{s}(z)$, corresponding to the 5th, 6th, and 7th rows of $\boldsymbol{\alpha}$, is obtained from

$$\frac{\partial}{\partial z}\begin{Bmatrix} \hat{\sigma}_{zz}(z) \\ \hat{\sigma}_{yz}(z) \\ \hat{\sigma}_{xz}(z) \end{Bmatrix} = \boldsymbol{\alpha}|_{5:7}^{:}\,\mathbf{s}(z). \tag{40}$$

From the left-hand side of Eq. (16)

$$\nabla\cdot\hat{\boldsymbol{\sigma}}^s(z) = \mathbf{A}'\hat{\boldsymbol{\sigma}}^s(z) + \mathbf{B}'\frac{\partial}{\partial z}\hat{\boldsymbol{\sigma}}^s(z), \tag{41}$$

where

$$\mathbf{A}' = \begin{bmatrix} -\imath k_x & 0 & 0 & 0 & 0 & -\imath k_y \\ 0 & -\imath k_y & 0 & 0 & 0 & -\imath k_x \\ 0 & 0 & 0 & -\imath k_y & -\imath k_x & 0 \end{bmatrix}, \tag{42}$$

and

$$\mathbf{B}' = \begin{bmatrix} 0 & 0 & 0 & 0 & 1 & 0 \\ 0 & 0 & 0 & 1 & 0 & 0 \\ 0 & 0 & 1 & 0 & 0 & 0 \end{bmatrix}. \tag{43}$$

Substituting Eqs. (41) and (31) in Eq. (16), the term $\boldsymbol{\alpha}|_{5:7}^{:}$ can be expressed as

$$\boldsymbol{\alpha}|_{5:7}^{:} = [\mathbf{B}'|_{:}^{3:5}]^{-1}[-\omega^2\tilde{\boldsymbol{\rho}}_s\mathbf{T}^{\mathbf{u}^s} - \omega^2\tilde{\boldsymbol{\rho}}_{eq}\tilde{\boldsymbol{\gamma}}\mathbf{T}^{\mathbf{u}^t} - \mathbf{A}'\hat{\mathbf{H}}^s(\mathbf{A}\mathbf{T}^{\mathbf{u}^s} + \mathbf{B}\boldsymbol{\alpha}|_{1:3}^{:})]. \quad (44)$$

4. Gradient of pressure, $\frac{\partial p(z)}{\partial z}$

What remains is the relation

$$\frac{\partial p(z)}{\partial z} = \boldsymbol{\alpha}|_{8}^{:}\,\mathbf{s}(z), \quad (45)$$

which can be directly determined by inserting Eqs. (26) and (35) into Eq. (17). Thus, the term $\alpha|_{8}^{:}$ in Eq. (45) may be expressed as

$$\boldsymbol{\alpha}|_{8}^{:} = -\omega^2\tilde{\boldsymbol{\rho}}_{eq}|_{3}^{:}\tilde{\boldsymbol{\gamma}}\mathbf{T}^{\mathbf{u}^s} - \omega^2\tilde{\boldsymbol{\rho}}_{eq}|_{3}^{:}\,\mathbf{T}^{\mathbf{u}^t}. \quad (46)$$

III. DISSIPATED AND KINETIC POWERS

To calculate the internal powers $\mathcal{P}$ of a layer, the integral associated with the scalar product of two complex quantities $f(z)$ and $g(z)$ has to be calculated according to

$$\mathcal{P} = \int_0^d f^*(z)g(z)\mathrm{d}z, \quad (47)$$

where d is the thickness of the layer and $f^*(z)$ denotes the complex conjugate of $f(z)$. An advantage of the proposed method is that $f(z)$ and $g(z)$ each may be expressed as a linear combination of the state variables in $\mathbf{s}(z)$, e.g. $f(z) = \mathbf{T}^f\,\mathbf{s}(z)$ and $g(z) = \mathbf{T}^g\,\mathbf{s}(z)$. Similarly, their spatial derivatives may be expressed as a linear combination of $\boldsymbol{\alpha}$, see, for example, Eq. (45).

To facilitate the calculations of the required integrals, following Eq. (11), the state variable amplitudes are expanded in terms of the wave contributions $\mathbf{q}$, the polarisation vectors $\boldsymbol{\Phi}$, and the diagonal wavenumber exponential matrix $\boldsymbol{\Lambda}(z)$. Thus, the integration over two arbitrary points can be rewritten in terms of wave properties and contributions

$$\mathcal{P} = \mathbf{q}^*\left[\int_0^d \boldsymbol{\Lambda}^*(z)\boldsymbol{\Phi}^*\mathbf{T}^{f*}\mathbf{T}^g\boldsymbol{\Phi}\boldsymbol{\Lambda}(z)\mathrm{d}z\right]\mathbf{q}. \quad (48)$$

Introducing $\boldsymbol{\Xi}\{\mathcal{P}\} = \mathbf{T}^{f*}\mathbf{T}^g$, where the matrix $\boldsymbol{\Xi}$ holds the contribution of the different state variables involved

$$\mathcal{P} = \mathbf{q}^*\left[\int_0^d \boldsymbol{\Lambda}^*(z)\boldsymbol{\Phi}^*\boldsymbol{\Xi}\{\mathcal{P}\}\boldsymbol{\Phi}\boldsymbol{\Lambda}(z)\mathrm{d}z\right]\mathbf{q}. \quad (49)$$

It is important to note that the quadratic factor $\boldsymbol{\Xi}\{\mathcal{P}\}$ depends on the nature of the medium, but not on its boundary conditions or the layer thickness.

As an example, a partial contribution to the time-averaged dissipated power, by shear deformation in the xz-plane of an anisotropic poroelastic material layer of thickness d placed at the origin of a Cartesian coordinate system, is given by

$$\Pi_{xz}^s = \mathrm{Re}\left\{\frac{\imath\omega}{4}\int_0^d \hat{\sigma}_{xz}^{s*}(z)\epsilon_{xz}^s(z)\mathrm{d}z\right\}, \quad (50)$$

where $\hat{\sigma}_{xz}^s(z)$ and $\epsilon_{xz}^s(z)$ are, respectively, the shear stress and shear strain in the solid frame of the poroelastic layer in the $x0z$-plane. The shear strain $\epsilon_{xz}^s(z)$ is given by

$$\epsilon_{xz}^s(z) = \frac{1}{2}\left[-\imath k_x u_z^s(z) + \frac{\partial u_x^s(z)}{\partial z}\right]. \quad (51)$$

As can be seen in Eq. (21), the fields $\hat{\sigma}_{xz}^s$, $u_x^s(z)$, and $u_z^s(z)$ are included in the state vector $\mathbf{s}(z)$. As a consequence of the wave expansion approach in Eq. (11), the state variable amplitude $u_z^s(z)$ may be computed by multiplying Eq. (11) by a the 3rd row of the Boolean matrix $\mathbf{T}^{\mathbf{u}^s}$ in Eq. (26)

$$u_z^s(z) = \mathbf{T}^{\mathbf{u}^s}|_3^{:}\,\boldsymbol{\Phi}\boldsymbol{\Lambda}(z)\mathbf{q}. \quad (52)$$

The shear stress $\hat{\sigma}_{xz}^s$ is then expressed via the 3rd row of the Boolean matrix $\mathbf{T}^{\hat{\boldsymbol{\sigma}}^s}$ in Eq. (25)

$$\hat{\sigma}_{xz}^s(z) = \mathbf{T}^{\hat{\boldsymbol{\sigma}}^s}|_3^{:}\,\boldsymbol{\Phi}\boldsymbol{\Lambda}(z)\mathbf{q}. \quad (53)$$

In a similar way, the partial derivative over z of $u_x(z)$ may be computed by introducing Eq. (11) into Eq. (2), and by multiplying with 1st row of the Boolean matrix $\mathbf{T}^{\mathbf{u}^s}$ in Eq. (26)

$$\frac{\partial u_x^s(z)}{\partial z} = -\mathbf{T}^{\mathbf{u}^s}|_1^{:}\boldsymbol{\alpha}\boldsymbol{\Phi}\boldsymbol{\Lambda}(z)\mathbf{q}. \quad (54)$$

Thus, Eq. (50) can be rewritten as a function of the exponential diagonal matrix of wavenumbers $\boldsymbol{\Lambda}(z)$, the polarisations $\boldsymbol{\Phi}$, and the wave contributions $\mathbf{q}$, as

$$\Pi_{xz}^s = \mathrm{Re}\left\{\mathbf{q}^*\left[\int_0^d \boldsymbol{\Lambda}^*(z)\boldsymbol{\Phi}^*\boldsymbol{\Xi}\{\Pi_{xz}^s\}\boldsymbol{\Phi}\boldsymbol{\Lambda}(z)\mathrm{d}z\right]\mathbf{q}\right\}, \quad (55)$$

with

$$\boldsymbol{\Xi}\{\Pi_{xz}^s\} = \frac{\imath\omega}{4}\left[\mathbf{T}^{\hat{\boldsymbol{\sigma}}^s}|_3^{:}\right]^*\left[\imath k_x\mathbf{T}^{\mathbf{u}^s}|_3^{:} + \mathbf{T}^{\mathbf{u}^s}|_1^{:}\,\boldsymbol{\alpha}\right]. \quad (56)$$

A similar procedure may be thus be applied in order to obtain the internal power associated to any other pair of complex quantities $f(z)$ and $g(z)$.

IV. APPLICATION AND RESULTS

A. Study case

To illustrate the application of the proposed method, a sandwich panel with two solid face sheets and a single porous core, i.e., Fig. 1 with N = 3, is investigated. The poroelastic core is anisotropic in the elastic and the acoustic properties, all sharing the same principal directions, and the influence of the directional properties is illustrated through a comparative study of different orientations of the porous material coordinate system.

The face sheets are 1 mm-thick isotropic aluminium layers, and the core material is an anisotropic anelastic melamine foam of thickness $d_{core} = 88$ mm. The acoustic

performance will be evaluated in terms of the transmission loss (TL) of the panel which is obtained from the pressure radiated by the solid face sheet opposite to the surface excited by the incident acoustic wave. The method to compute the TL is given in Ref. 22, where it is detailed how the transmitted pressure field can be evaluated.

Table I summarises the values of the material parameters used in the application. The anisotropic material parameters of the melamine foam in the core are taken from recently published works and are here given in the material coordinate system of the foam $(0, x', y, z')$, as defined in Fig. 2. The flow resistivity tensor, was estimated by Van der Kelen *et al.*[27] (in Pa s m^{-2}), as

$$\boldsymbol{\sigma}_{\text{flow}} = \begin{bmatrix} 0.9727 & 0 & 0 \\ & 1.0655 & 0 \\ \text{sym.} & & 1.1318 \end{bmatrix} \times 10^4, \tag{57}$$

and the Hooke's matrix was estimated by Cuenca *et al.*[5] ($\times 10^5$ Pa) as

$$\hat{\mathbf{C}} = \begin{bmatrix} 7.7194 & 3.4252 & -0.0226 & 0 & 0 & 0 \\ & 4.2782 & 1.1845 & 0 & 0 & 0 \\ & & 2.2155 & 0 & 0 & 0 \\ & & & 1.0364 & 0 & 0 \\ & \text{sym.} & & & 1.2368 & 0 \\ & & & & & 1.0123 \end{bmatrix}. \tag{58}$$

The transformations used to rotate the material natural coordinate system are detailed in Cuenca *et al.*[5] In what follows, the angle β corresponds to the direct rotation around the $(0y)$ axis of the material coordinate system of the foam, see Fig. 2. Note that, in the unrotated state, the material coordinate system is aligned with the global coordinate system and the material properties are orthotropic.

To highlight the particular mechanisms related to the dynamics of an anisotropic material in a multilayered system, results for an isotropic equivalent core are also given. The corresponding isotropic material parameters were computed using the method proposed by Norris[28] and are given in Table I.

TABLE I. Parameters of the aluminium sheets and of the melamine foam used for the application.

Parameter	Symbol	Value
Aluminium sheets		
Density	ρ^e	2700 kg m^{-3}
Young's modulus	E	7×10^{10} Pa
Loss factor	η	0.01
Poisson ratio	ν	0.3
Melamine foam		
Tortuosity	α_t	1.2
Viscous charac. length	Λ	240×10^{-6} m
Thermal charac. length	Λ'	490×10^{-6} m
Porosity	ϕ	0.99
Density of frame	ρ_1	9.2 kg m^{-3}
Fractional derivative order	$\hat{\alpha}$	0.33348
Relaxation frequency	$\hat{\beta}$	812.69×10^3 rad s^{-1}
Anelastic contribution	$\hat{b}$	0.29620
Isotropic equivalent foam		
Young's modulus	E_{iso}	3.155×10^5 Pa
Viscous loss factor	η_{elastic}	0.032
Poisson ratio	ν_{iso}	0.285
Flow resistivity	$\sigma_{\text{iso}}^{\text{flow}}$	1.0567×10^4 Pa s m^{-2}

B. Transmission loss

The dynamic behaviour will be discussed in three defined frequency ranges: low, $f \sim [100 - 500]$ Hz, mid, $f \sim [0.5 - 1]$ kHz, and high, $f \sim [1 - 5]$ kHz. Two different excitations are used, one for normal incidence, $\theta_1 = 0$ deg, $\theta_2 = 0$deg, and one for oblique incidence, $\theta_1 = 45$deg, $\theta_2 = 50$deg. For the normal incidence case, the material coordinate transformations are symmetric with respect to $\beta = 0$ rad and $\beta = \pi/2$ rad, while for the oblique incidence this is no longer the case.

The TL under normal incidence is shown as a function of frequency in Fig. 3(a) for 3 different rotations of the porous material coordinate system, $\beta = [0; \pi/4, \pi/2]$ rad, together with the TL of the closest isotropic equivalent material model, and for oblique incidence in Fig. 3(b), for 4 different rotations of the porous material coordinate system, $\beta = [0; \pi/4, \pi/2; 3\pi/4]$ rad.

The low frequency response is for both excitations characterised by resonances and anti-resonances that depend on the rotation angle β. Similarly, the high frequency response

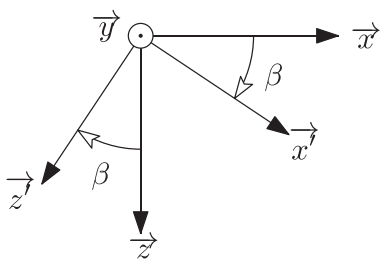

FIG. 2. Global coordinate system $(0, x, y, z)$, foam material reference system $(0, x', y, z')$, and definition of rotation angle β.

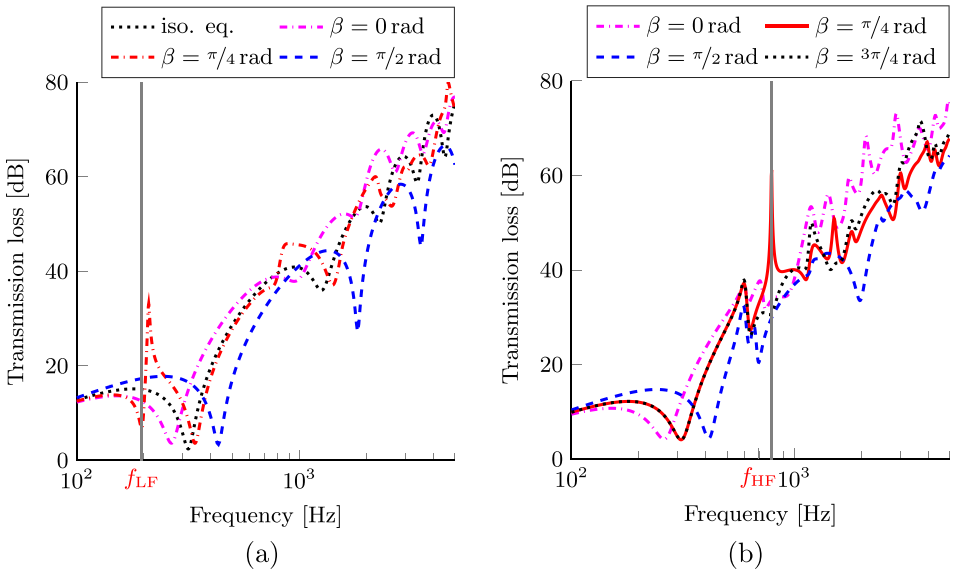

FIG. 3. Acoustic transmission loss of the multilayered structure excited by a plane wave as a function of frequency; (a) under normal incidence ($\theta_1 = 0$deg, $\theta_2 = 0$deg), and (b) under oblique incidence ($\theta_1 = 45$deg, $\theta_2 = 50$deg).

of the multilayered system exhibits a resonant behaviour with an apparent level of damping dependent on β.

For the normal incidence, a resonance and anti-resonance appear in the TL at $f = f_{LF} = 195.7$ Hz, see Fig. 3(a), for material rotations around $\beta \sim \pi/4$ rad which is neither present for the other rotations nor for the oblique incidence excitation. In the medium frequency range and the oblique incidence excitation, anti-resonances depending on the rotation angle β may be observed.

In addition, the response predicted using the material properties according to the closest isotropic equivalent is very similar to the normal incidence results for $\beta = \pi/4$ rad.

C. Kinetic powers

To analyse the complex interactions induced by the anisotropic poroelastic core, the internal powers may be calculated as functions of frequency and material coordinate rotations. As an example, from Eq. (49), the total kinetic powers of the porous core can be calculated. The results obtained for 3 material coordinate rotations, are shown in Fig. 4 under normal incidence.

It can be observed that the overall kinetic power of the porous material is predominantly governed by the motion in z for the three material coordinate rotations. Also, the kinetic power due to motion in y is negligible for all material rotations under normal incidence. In contrast, the kinetic power related to the motion in x has a significant contribution for $\beta = \pi/4$ rad, around $f \sim f_{LF}$, whereas it has little contribution to the overall kinetic power when the material coordinate system is aligned with the global, i.e., $\beta = 0$ rad and $\beta = \pi/2$ rad.

V. DISCUSSION

The focus of the present work is set on the method proposed for solving the anisotropic multilayer transmission problem and their ability to provide an interpretation of the mechanisms governing the acoustic performance of confined anisotropic poroelastic media dynamics. Thus, in the discussion the performance as such will not be discussed except

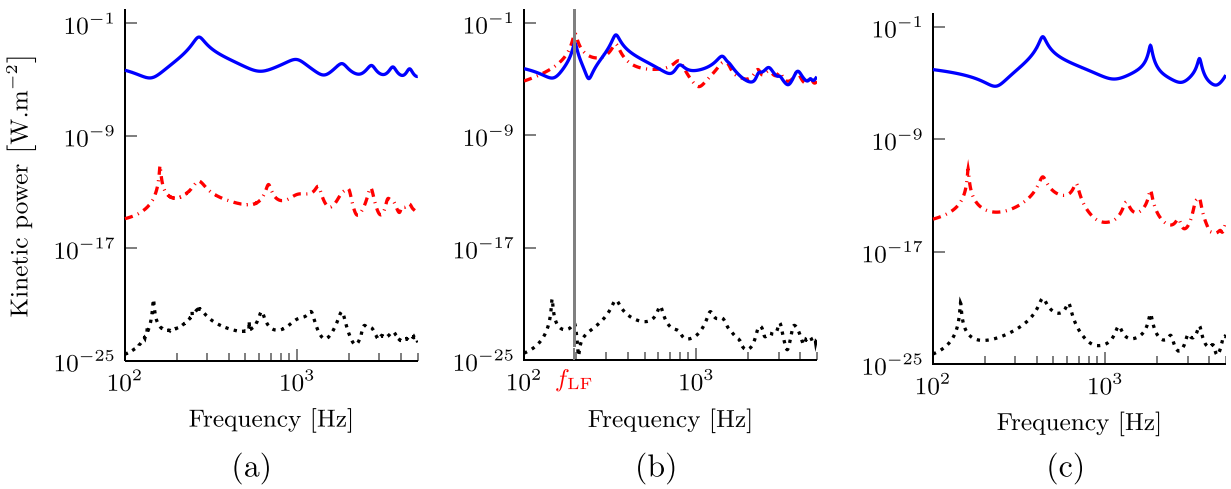

FIG. 4. Total kinetic power within the poroelastic core layer under normal incidence for different rotations of the material coordinates. Legend: red dot-dashed line, projection on x; black dotted line, projection on y; blue solid line, projection on z. (a) $\beta = 0$ rad, (b) $\beta = \pi/4$ rad, and (c) $\beta = \pi/2$ rad.

when used to show in which ways the method may be utilised in the analysis. In particular, the dependence of the response on the rotation angle, the underlying mechanisms controlling the frequency shift of the fundamental resonance, and the appearance of resonances and anti-resonances in the low and mid-frequency ranges, will be highlighted.

A. Fundamental resonance frequency shift under normal incidence

The strong dependence of the normal incidence TL on the rotation angle β, see Fig. 3(a), is related to the mechanical stiffness of the material in compression in the z-direction. More specifically, it is the variation of the foam's Hooke's tensor component $\hat{H}^s_{33}$, as a function of β, which governs the phase velocity of the compressional deformation. This is evident from, Fig. 5, which shows the variation of the resonance frequency and $\sqrt{\hat{H}^s_{33}}$. This, together with the closely related responses obtained using the material properties according to the closest isotropic equivalent and $\beta = \pi/4$ rad, will be further discussed below.

In order to understand this behaviour, the contribution $\mathbf{q}$ of each wave in the porous material to the response, see Eq. (11), is presented in Fig. 6, together with the wave contributions of the closest isotropic equivalent, at $f = 339.7$ Hz. Note that the response is dominated by the same set of waves in both cases, $\boldsymbol{\psi}_3$ and $\boldsymbol{\psi}_4$, thus confirming the observed dependence on $\hat{H}^s_{33}$ and providing support for an explanation of the similarities between the closest isotropic equivalent model and the $\beta = \pi/4$ rad. The fundamental resonance then corresponds to the phenomenon which is characterised as a "breathing" motion in the case of isotropic multilayered systems. Due to the anisotropy, there is a non-negligible influence of other types of deformation waves in the poroelastic medium studied in the current case, hence the term fundamental resonance will be used in the paper.

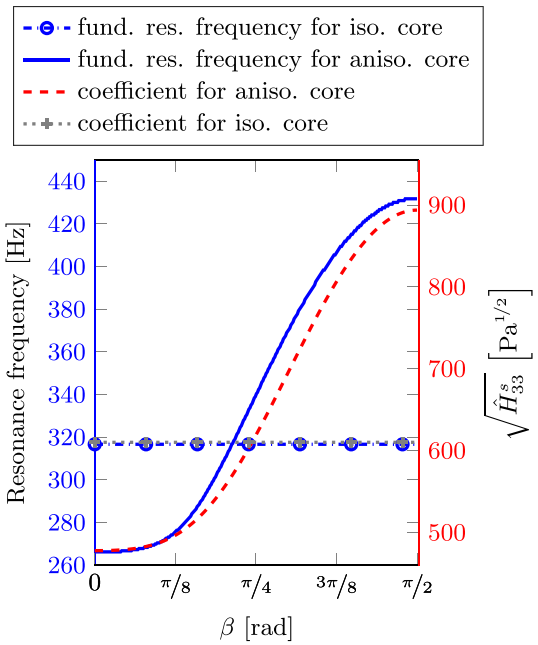

FIG. 5. Fundamental resonance frequency of the sandwich panel under normal incident plane wave, and coefficient $\sqrt{\hat{H}^s_{33}}$ of the poroelastic material, as functions of β.

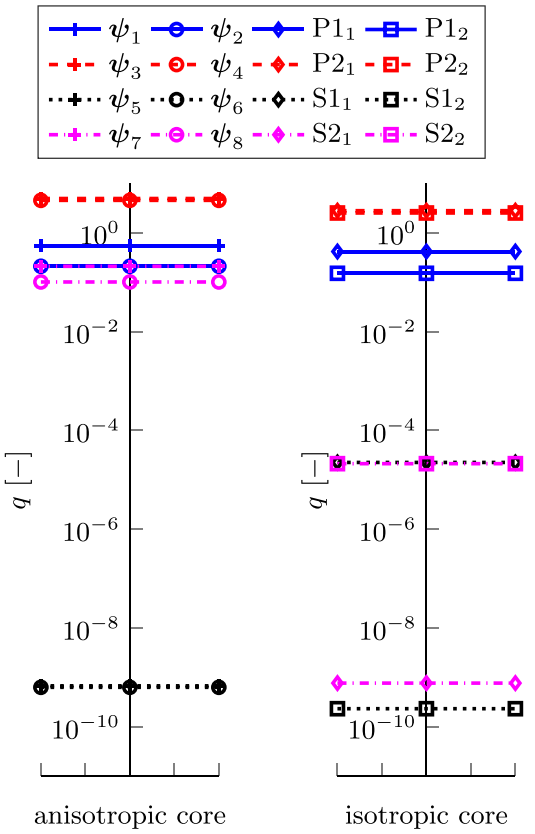

FIG. 6. Wave contributions at $f = 339.7$ Hz under normal incident acoustic excitation of the different waves in the core in (left) the panel with anisotropic poroelastic core for $\beta = \pi/4$ rad, and (right) the panel with closest isotropic equivalent poroelastic core.

B. Low frequency resonance and anti-resonance under normal incidence

There is one observed response that stands out for material rotations around $\beta \sim \pi/4$ rad and normal incidence excitation. At $f = f_{LF} = 195.7$ Hz, see Fig. 3(a), a resonance and anti-resonance appear in the TL which are neither present in the other cases nor for the results pertaining to the closest isotropic equivalent. At this particular frequency and material coordinate rotation, the displacement field in the poroelastic core is dominated by a motion in the x-direction, see Fig. 4 at $f \sim f_{LF}$.

To further explain this, the contributions of the individual waves in Eq. (11), q_i, are shown in Fig. 7(a) as a function of the relative alignment at $f = f_{LF}$ for the range $\beta = [0, \pi/2]$ rad. For angles where the material coordinate system is aligned with the global coordinate system, i.e., $\beta = 0$ rad and $\beta = \pi/2$ rad, the $\boldsymbol{\psi}_3$ and $\boldsymbol{\psi}_4$ waves dominate the behaviour of the layer. In contrast, for $\beta \sim [\pi/8, 3\pi/8]$ rad, the behaviour of the layer is governed by the $\boldsymbol{\psi}_7$ and $\boldsymbol{\psi}_8$ waves in the porous medium, with some contribution of the $\boldsymbol{\psi}_1$, $\boldsymbol{\psi}_2$, $\boldsymbol{\psi}_3$, and $\boldsymbol{\psi}_4$ waves. At the same time, the overall contribution of the $\boldsymbol{\psi}_5$ and $\boldsymbol{\psi}_6$ waves is negligible for material coordinate rotations.

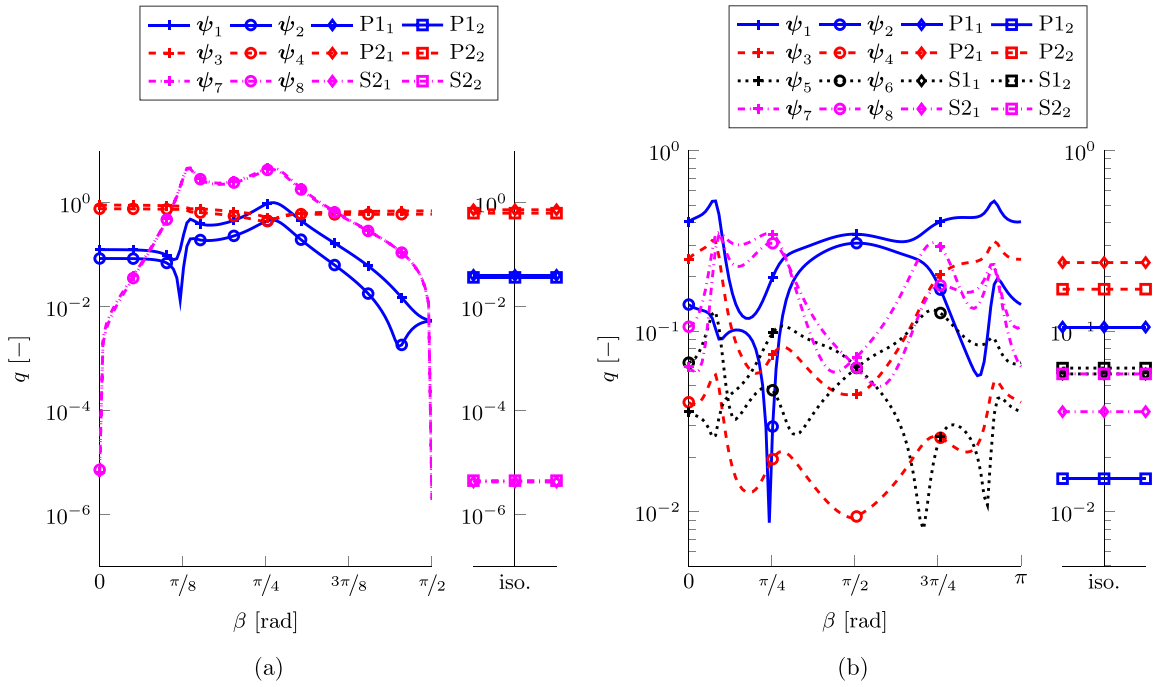

FIG. 7. Wave contributions of the waves in the anisotropic core and of the waves in the closest isotropic equivalent core. (a) $f = f_{\mathrm{LF}} = 195.7$ Hz (left) Multilayered panel with anisotropic porous core, (right) with closest isotropic equivalent core, under normal incident acoustic excitation. (b) $f = f_{\mathrm{HF}} = 792.4$ Hz (left) Multilayered panel with anisotropic porous core, (right) with closest isotropic equivalent core, under oblique incident excitation.

For comparison, the wave contributions in the same system composed with the closest isotropic equivalent porous core, for $f = f_{\mathrm{LF}}$ are also shown in Fig. 7(a). In this case, the response is governed by the contributions of the waves P2$_1$ and P2$_2$, while the other waves have a negligible contribution to the behaviour of the material under normal incidence.

C. Mid-frequency anti-resonances at oblique incidence

For oblique incidence, anti-resonances appear in the TL in the mid frequency range, Fig. 3(b). Although these appear for all material coordinate rotations, they are particularly strong for the $\beta = 3\pi/4$ rad results. The wave contributions q_i at $f = f_{\mathrm{HF}}$ are shown in Fig. 7(b). For $\beta \sim [3\pi/8, 5\pi/8]$ rad, the response is dominated by the $\boldsymbol{\psi}_7$ and $\boldsymbol{\psi}_8$ waves. The effects of this unsymmetric excitation are particularly reflected in the wave contributions at $\beta = 3\pi/4$ rad. While the TL at this frequency shows a similar magnitude as $\beta = \pi/4$ rad, see Fig. 3(b), the response is clearly controlled by a different set of waves ($\boldsymbol{\psi}_1$), see Fig. 7(b).

D. Wave analysis

As previously discussed, particular waves dominate the behaviour of the confined anisotropic poroelastic medium. The proposed solution method may be used to characterise these in more depth, thus, allowing for an analysis of the inherent physical phenomena governing the response of anisotropic poroelastic materials. One such evaluation is to calculate the amount of shear deformation a certain wave represents for different material coordinate rotations.

This may be computed from Eq. (23), and as an example, for normal incidence and thus $k_x = k_y = 0$, the ratio Ω_{xz} between the shear strain in the xz-plane and the sum of strains may be computed from the free waves used in the solution (11)

$$\Omega_{xz}^{i} = \left| \frac{\epsilon_{xz}(\boldsymbol{\psi}_i)}{\sum_{k,l=x,y,z} \epsilon_{kl}(\boldsymbol{\psi}_i)} \right| \tag{59}$$

$$= \left| \frac{\boldsymbol{\Phi}|_1^i}{\boldsymbol{\Phi}|_1^i + \boldsymbol{\Phi}|_2^i + 2\boldsymbol{\Phi}|_3^i} \right|, \tag{60}$$

for $i = 1, \ldots, 8$, and where the convention introduced in Sec. II D is adopted.

As seen in Fig. 8, in the unrotated material states the wave field is clearly divided into purely compressional (P) and pure shear (S) waves. In contrast to this, for, e.g., $\beta = \pi/4$ rad, all the contributing waves induce both shear and compressional strains, which suggests a significant coupling between compressional and shear deformations for this material coordinate orientation. Note also that neither $\boldsymbol{\psi}_5$, $\boldsymbol{\psi}_6$, S1$_1$ nor S1$_2$ are shown as they have no shear strain component in the xz-plane under normal incidence.

The appearance of resonances and anti-resonances in the TL curves may be understood in terms of the wavelengths, which may be computed from Eq. (14). Fig. 9 presents the wavelengths of each wave in the anisotropic melamine foam for two material coordinate rotations, $\beta = [\pi/4; 3\pi/4]$ rad, as a function of frequency for a plane wave under oblique incidence. For both material rotations, the wavelength difference between waves of the same nature is negligible relative to the wavelengths. Therefore, Fig. 9 is representative of the wavelengths in both material coordinate system rotations. Assuming an incident wave at an angle θ_1 in a multilayered system with a confined poroelastic core, standing waves may

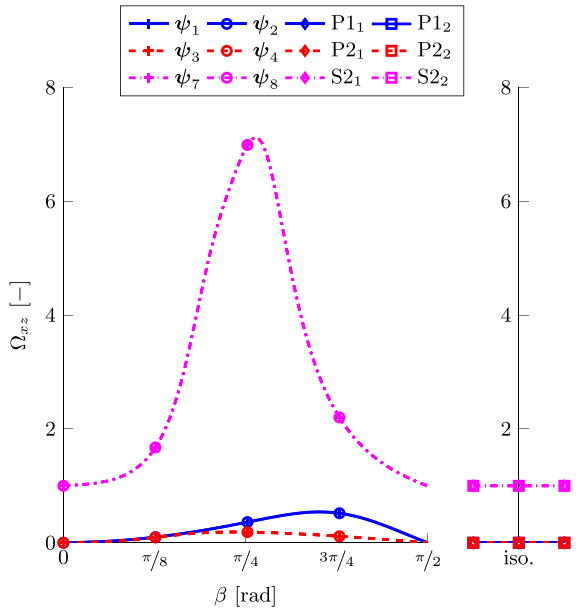

FIG. 8. Eq. (60) evaluated for normal incidence and $f = f_{\mathrm{LF}}$ in (left) the waves in the anisotropic core as a function of the rotational angle β, and (right) the waves in the closest isotropic equivalent core.

possibly form as the wavelengths of the waves governing the behaviour of the system matches a multiple of the length $L_{\theta_1} = d_{\mathrm{core}}/\cos(\theta_1)$.

Using this relation, the horizontal solid line in Fig. 9 is calculated as $2L_{\theta_1}$ for $\theta_1 = 45$deg. The frequency where this line coincide with the dispersion curves for the dominant wave, $\boldsymbol{\psi}_7$, f_{HF}, corresponds to the frequency at which the high amplitude anti-resonance appears in the TL for $\beta = \pi/4$ rad, see Fig. 3(b). In contrast, for $\beta = 3\pi/4$ rad, this wave is not dominating the response of the system, thus the length matching does not significantly affect the TL.

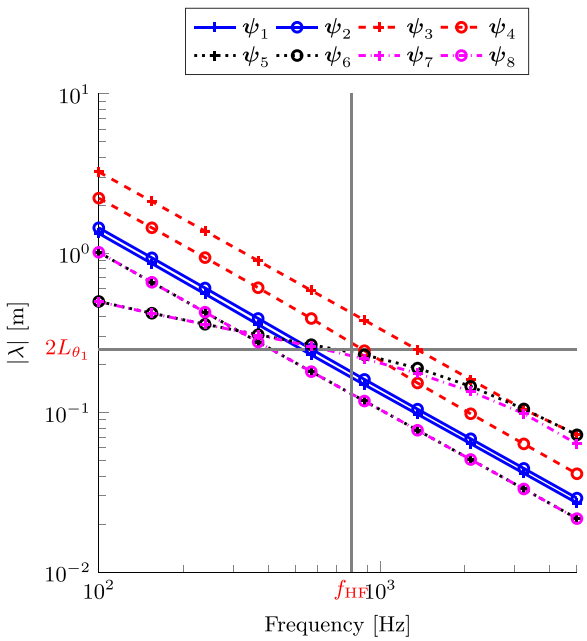

FIG. 9. Absolute value of the wavelengths of the different waves in the porous media under oblique incidence ($\theta_1 = 45\,\mathrm{deg}\,\theta_2 = 50\,\mathrm{deg}$) as a function of frequency under oblique incidence for $\beta = [\pi/4, 3\pi/4]$ rad.

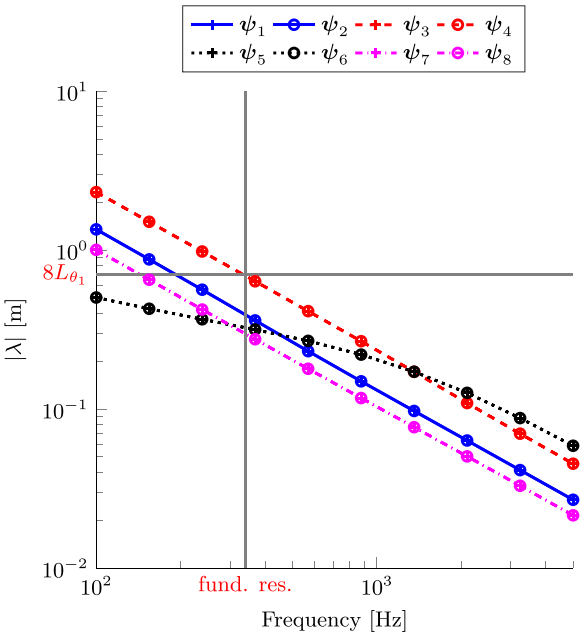

FIG. 10. Absolute values of the wavelengths of the different waves in the porous media under normal incidence ($\theta_1 = 0\,\mathrm{deg}\,\theta_2 = 0\,\mathrm{deg}$) as a function of frequency under normal incidence for $\beta = \pi/4$ rad.

In a similar manner, for the case under normal incidence, this method allows to predict the frequency of the fundamental resonance. As an example, for $\beta = \pi/4$ rad this occurs when the wavelength of $\boldsymbol{\psi}_3$ and $\boldsymbol{\psi}_4$ matches the length $8L_{\theta_1}$, as seen in Fig. 10.

VI. CONCLUSION

The proposed method allows for a deep analysis of the intrinsic mechanisms of the dynamic behaviour of confined anisotropic poroelastic media in a semi-infinite multilayered system. The assumed solution, based on plane wave expansion and formulated according to Stroh, fills a previous lack of computational methods for generally poroelastic anisotropic media. Analysing the wave properties and the wave contributions highlights the influence of intrinsic anisotropic phenomena, such as shear- compression coupling related to the material alignment, which is verified by the total kinetic powers in the media. As a consequence, for certain material orientations, significant anti-resonances appear in the TL curve.

Furthermore, the dynamic response exhibits a strong dependence on the material orientation of fully anisotropic porous materials, with significant frequency shifts in the fundamental resonance. These are shown to be related to the variation of mechanical compression moduli. The analysis shows that these variations induce a shift of the geometrical coincidence frequency of a set of dominant waves in the anisotropic porous medium.

The method is generally applicable to arbitrary multilayered configurations with mixed coupling conditions under arbitrary acoustic plane wave excitation.

[1]J. Allard, R. Bourdier, and A. L'Esperance, J. Sound Vib. **114**, 233 (1987).
[2]H. J. Rice and P. Göransson, Int. J. Mech. Sci. **41**, 561 (1999).

[3]J. F. Allard, O. Dazel, J. Descheemaeker, N. Geebelen, L. Boeckx, and W. Lauriks, J. Appl. Phys. **106**, 014906 (2009).
[4]P. Göransson and N.-E. Hörlin, Acta Acust. Acust. **96**, 258 (2010).
[5]J. Cuenca, C. Van der Kelen, and P. Göransson, J. Appl. Phys. **115**, 084904 (2014).
[6]E. Lind Nordgren, P. Göransson, J.-F. Deü, and O. Dazel, J. Acoust. Soc. Am. **133**, EL426 (2013).
[7]M. A. Biot, J. Appl. Phys. **25**, 1385 (1954).
[8]M. A. Biot, J. Appl. Phys. **26**, 182 (1955).
[9]M. A. Biot, J. Acoust. Soc. Am. **28**, 168 (1956).
[10]M. A. Biot, J. Appl. Phys. **33**, 1482 (1962).
[11]R. Lewis and B. Schrefler, *Finite Element Method in the Deformation and Consolidation of Porous Media* (John Wiley and Sons Inc., New York, NY, 1998).
[12]A. Gajo, A. Saetta, and R. Vitaliani, Int. J. Numer. Methods Eng. **37**, 1231 (1994).
[13]N.-E. Hörlin and P. Göransson, Int. J. Numer. Methods Eng. **84**, 1519 (2010).
[14]L. Sanchez-Ricart and J. García-Peláez, Meccanica **49**, 2757 (2014).
[15]P. J. Matuszyk and L. F. Demkowicz, Comput. Methods Appl. Mech. Eng. **281**, 54 (2014).
[16]M. Sharma, Geophys. J. Int. **156**, 329 (2004).
[17]J. M. Carcione, *Wave Fields in Real Media*, Handbook of Geophysical Exploration (Burlington Pergamon, Burlington, 2007).
[18]J. M. Carcione, D. Gei, and S. Treitel, Geophysics **75**, T37 (2010).
[19]J. M. Carcione, Proc. Math. Phys. Eng. Sci. **457**, 331 (2001).
[20]P. Khurana, L. Boeckx, W. Lauriks, P. Leclaire, O. Dazel, and J. F. Allard, J. Acoust. Soc. Am. **125**, 915 (2009).
[21]C. Baron and S. Naili, C. R. Méc. **336**, 722 (2008).
[22]O. Dazel, J.-P. Groby, B. Brouard, and C. Potel, J. Appl. Phys. **113**, 083506 (2013).
[23]Q. Serra, M. N. Ichchou, and J.-F. Deü, J. Comput. Acoust. **23**, 1550020 (2015).
[24]O. Dazel, B. Brouard, C. Depollier, and S. Griffiths, J. Acoust. Soc. Am. **121**, 3509 (2007).
[25]J. Cuenca and P. Göransson, J. Acoust. Soc. Am. **132**, 621 (2012).
[26]J. F. Allard and N. Atalla, *Propagation of Sound in Porous Media: Modelling Sound Absorbing Materials*, 2nd ed. (John Wiley & Sons, 2009), pp. 1–358.
[27]C. Van der Kelen and P. Göransson, J. Acoust. Soc. Am. **134**, 4659 (2013).
[28]A. N. Norris, J. Mech. Mater. Struct. **1**, 223 (2006).